Published in final edited form as:
Dev Biol. 2010 August 1; 344(1): 259–271. doi:10.1016/j.ydbio.2010.05.007.

A Transitional Extracellular Matrix Instructs Cell Behavior During Muscle Regeneration

Sarah Calve[a], **Shannon J. Odelberg**[b], and **Hans-Georg Simon**[a]

[a] Department of Pediatrics, Northwestern University, The Feinberg School of Medicine, Children's Memorial Research Center, 2300 Children's Plaza, Chicago, IL 60614.

[b] Department of Internal Medicine, Division of Cardiology, University of Utah, Salt Lake City, UT 84132. sodelber@genetics.utah.edu

Abstract

Urodele amphibians regenerate appendages through the recruitment of progenitor cells into a blastema that rebuilds the lost tissue. Blastemal formation is accompanied by extensive remodeling of the extracellular matrix. Although this remodeling process is important for appendage regeneration, it is not known whether the remodeled matrix directly influences the generation and behavior of blastemal progenitor cells. By integrating *in vivo* 3-dimensional spatiotemporal matrix maps with *in vitro* functional time-lapse imaging, we show that key components of this dynamic matrix, hyaluronic acid, tenascin-C and fibronectin, differentially direct cellular behaviors including DNA synthesis, migration, myotube fragmentation and myoblast fusion. These data indicate that both satellite cells and fragmenting myofibers contribute to the regeneration blastema and that the local extracellular environment provides instructive cues for the regenerative process. The fact that amphibian and mammalian myoblasts exhibit similar responses to various matrices suggests that the ability to sense and respond to regenerative signals is evolutionarily conserved.

Keywords

Extracellular matrix; time-lapse microscopy; 3D imaging; skeletal muscle progenitor cells; limb regeneration; newt

Introduction

Tissues severely traumatized by injury or disease present significant problems to both the physician and the affected individual because the wound is typically repaired with scar tissue, often resulting in suboptimal restoration of tissue architecture and function. In contrast, complete functional repair of damaged or lost structures has been demonstrated in many animal phyla, and tissue regeneration is probably a basal metazoan character that has

Correspondence to: Sarah Calve.

Correspondence to: Dr. H.-G. Simon, Northwestern University, The Feinberg School of Medicine, Children's Memorial Research Center (CMRC), 2300 Children's Plaza M/C 204, Chicago, IL 60614, USA, Tel: 773-755-6391, Fax: 773-755-6385, hgsimon@northwestern.edu. s-calve@northwestern.edu.

been lost in mammals (Alvarado, 2000). Among vertebrates, newts and other urodele amphibians have retained the ability to completely regenerate injured tissues and lost appendages without scar formation. During regeneration, it is thought that multipotent progenitor cells are recruited from differentiated tissues close to the wound site. These stem-like cells give rise to a regenerative blastema that rebuilds tissues complete with muscles, bones and nerves (Carlson, 1970; Hay and Fischman, 1961; Iten and Bryant, 1973; Namenwirth, 1974; Oberpriller and Oberpriller, 1974).

Early studies using the regenerating amphibian limb model indicated that injured multinucleate myofibers can dedifferentiate into mononucleate cells and contribute to the regenerating blastema (Hay, 1959; Namenwirth, 1974). This concept was supported by cell lineage studies in which *in vitro* derived myotubes were labeled and transplanted into regenerating blastemas. *In vivo* tracing found that these myotubes fragmented into mononucleate progenitor cells, ultimately contributing to differentiated tissues of the regenerate (Kumar et al., 2000; Lo et al., 1993). Work on tail myofibers injured *in situ* also revealed evidence of progenitor cell generation via myofiber fragmentation (Echeverri and Tanaka, 2002). To decipher the molecular and cellular mechanisms behind the generation of progenitor cells, recent studies investigated the behavior of individual amphibian myofibers *in vitro*. Kumar et al. (2004) isolated axolotl skeletal muscle fibers and, by using lineage tracing and live cell imaging, they concluded that these myofibers are capable of fragmentation. In contrast, Morrison and colleagues (2006) showed that the multinucleate syncytium of newt myofibers remained intact when cultured *in vitro* and only observed activation of mononucleate satellite cells. These discrepancies may be grounded in the use of different animal models, but their experimental parameters are also distinct. While Kumar et al. (2004) utilized uncoated polystyrene dishes, Morrison et al. (2006) plated newt myofibers on dishes coated with Matrigel, a matrix isolated from murine EHS sarcoma cells rich in basement membrane components. However, neither study considered the dramatic remodeling of the extracellular matrix (ECM) that results from muscle injury in both regenerating and non-regenerating vertebrates nor how these changes may affect cell behavior.

The ECM of skeletal muscle is composed of the interstitial matrix and the basement membrane. The interstitial ECM consists of type I collagen, fibronectin (FN), hyaluronic acid (HA), chondroitin sulfate and dermatan sulfate proteoglycans, and fills the spaces between muscle fibers and their bundles while maintaining mechanical continuity with tendons (Grounds, 2008; Okita et al., 2004). Upon injury in mammals, the muscle degenerates and satellite cells associated with the myofibers are the main source of progenitor cells, which proliferate and differentiate to repair the damaged tissue (Seale et al., 2000). A local upregulation of HA, FN, and tenascin (TN) has been reported, but whether these ECM molecules directly affect muscle cell behavior during repair is not known (Donaldson et al., 1991; Goetsch et al., 2003; Grounds, 2008; Huijbregts et al., 2001; Hurme and Kalimo, 1992). The muscle basement membrane sheath is comprised predominantly of the network-forming collagens type IV and VI and laminin (Grounds, 2008; Sanes, 2003). When the muscle degenerates, the damaged basement membrane hull is left behind where it acts as a scaffold to direct myofiber fusion and is eventually repaired by the newly formed

muscle (Vracko and Benditt, 1972). Based on their structure-supporting nature, components of the basement membrane have been the focus of most studies investigating muscle repair (Boonen et al., 2009; Macfelda et al., 2007; Maley et al., 1995; Merritt et al., 2010).

During the early stages of regenerative repair in amphibians, ECM proteins typical of differentiated muscle, such as laminin and type I collagen, become downregulated (Gulati et al., 1983a; Mailman and Dresden, 1976). In contrast, HA, TN and FN are strikingly upregulated (Contreras et al., 2009; Onda et al., 1991; Repesh et al., 1982; Tassava et al., 1996; Toole and Gross, 1971). The expression of HA, TN and FN is reminiscent of embryogenesis, where they have been described as integral ECM components during developmental processes (Chiquet et al., 1981; Chiquet and Fambrough, 1984; Kosher et al., 1981; Matsumoto et al., 2009; Ros et al., 1995), suggesting that the production of a matrix rich in these molecules stimulates cellular responses that drive tissue formation. Our preliminary studies indicate that the ECM may influence myotube fragmentation (Calve and Simon, 2010) and that inhibition of ECM-modifying matrix metalloproteinases (MMPs) results in aberrant regeneration (Vinarsky et al., 2005).

Although ECM remodeling appears to be an essential requirement for normal appendage regeneration, it is not known how the composition of the transitional matrix changes with respect to skeletal muscle during the regeneration process and whether ECM molecules provide local instructive cues to myogenic progenitor cells. To gain insight into the biological significance of the transitional regenerative matrix, we characterized the dynamic changes in matrix composition at high resolution in 3D during newt forelimb regeneration and determined the functional roles of distinct ECM components on the behavior of newt and mouse muscle-derived cells using *in vitro* time-lapse microscopy.

Materials and Methods

Animal Care

Adult red spotted newts (*Notophthalmus viridescens*) were provided by Charles Sullivan Company, Inc. (Nashville, TN). Before surgery, newts were anesthetized with 0.1% ethyl 3-aminobenzoate methanesulfonate salt (Sigma) in 0.04% Instant Ocean (Aquarium Systems). Forelimbs were amputated proximal to the elbow and animals were allowed to recover in 0.25% sulfamerazine sodium salt (Sigma) in 0.04% Instant Ocean. Three hours before tissue harvest, newts were injected intraperitoneally with 100 μL 1 mM 5-ethynyl-2’-deoxyuridine (EdU, Invitrogen) in 0.8X phosphate buffered saline (PBS, Cellgro) to allow for the identification of cells that had reentered the cell cycle. Newts were re-anesthetized and regenerating limbs were harvested, imbedded in OCT, frozen in an isopentane-dry ice slurry and stored at -80°C.

Microarray Analysis

Custom microarrays were prepared by Agilent Technologies using data from both in-house DNA sequences and public databases. Each microarray represented 1,876 putative transcripts from 6 newt species with 93% of the transcript sequences being derived from *N. viridescens*. The majority of *N. viridescens* genes were cloned from mRNA isolated from

regenerating tissues. A 60-mer probe was designed for each transcript using Agilent eArray software and each probe was represented 23 times on a grid containing 44,000 oligonucleotide probes. Newt limbs were amputated through the stylopodium and tails were amputated 2 cm distal to the hindlimbs. RNA was isolated from regenerating tissues at 0, 1, 3, 6, 12, or 21 days postamputation. The Huntsman Cancer Institute Microarray Core Facility at the University of Utah prepared the RNA probes and performed the hybridizations. RNA probes were generated by amplifying the isolated RNA and labeling with Cy3 or Cy5. Microarrays were competitively hybridized with Cy5- and Cy3-labeled probes from regenerating and day 0 (intact) tissues. The microarrays were Lowess normalized, Cy5:Cy3 ratios (regenerating vs. intact tissues) for each hybridization were $\log_{10}$ transformed and the geometric means and standard deviations were obtained for repetitive hybridizations.

Immunohistochemistry

Serial cryosections of 16 μm, encompassing the full thickness of a limb, were collected. Sections were fixed in 4% paraformaldehyde (Sigma) for 5 minutes, rinsed in PBS, permeabilized with 0.1% Triton X-100 (Amersham Life Science) in PBS for 1 minute then rinsed with PBS. Sections were blocked for 30 minutes [blocking buffer: 20% goat serum (Invitrogen), 0.2% bovine serum albumin (BSA, Sigma), 50 mM ammonium chloride (Sigma), 25 mM glycine (Fisher), 25 mM lysine (Sigma), 0.02% sodium azide (Sigma) in PBS]. Primary antibodies were applied for 1 hour and sections were rinsed with 0.1% Tween-20 (Sigma) in PBS (Table S1). Slides were blocked again for 5 minutes before staining with the appropriate secondary detection reagents [Alexa Fluor (AF) 647 anti-mouse IgG2b (Invitrogen), AF546 anti-mouse IgG1, DyLight 649 anti-rabbit (Pierce), AF488 anti-mouse, AF546 streptavidin, DAPI (Roche)] for 30 minutes. Slides were rinsed with 0.1% Tween-20 in PBS and mounted with FLUORO-GEL (Electron Microscopy Sciences).

To visualize hyaluronic acid distribution, biotinylated hyaluronic acid binding protein (HABP, Calbiochem) was used as an indirect probe. After fixation and permeabilization, and prior to labeling sections with HABP, endogenous avidin and biotin activity was inactivated with an Avidin/Biotin blocking kit (Zymed Labs). Specificity was confirmed by preincubating HABP with a solution of 1 mg/mL hyaluronic acid sodium salt (HA, MW = 5.0×10^5 – 1.2×10^6, Calbiochem), and we observed endogenous avidin and/or biotin staining in the epidermis (e), consistent with previous reports (data not shown) (Epperlein et al., 2000). To identify cells that incorporated EdU, a cell-permeable dye-azide was conjugated to EdU via a copper catalyzed click-chemistry reaction (Salic and Mitchison, 2008). Briefly, after fixation, permeabilization and blocking, sections were incubated for 30 minutes with AF488 conjugated azide (Invitrogen) diluted 1:500 in 0.1 M Tris (pH 8.5, Fisher), 1 mM copper (II) sulfate (Sigma) and 0.1 M ascorbic acid (Sigma).

Imaging and 3D Rendering

For efficient processing of the 70 – 100 sections representative of the complete thickness of a regenerating newt forelimb, an Intavis InsituPro robot was utilized. Sections were imaged at 5x using a Leica DMI6000 microscope controlled with Image-ProPlus Advanced

Microscopy Suite (Media Cybernetics). Custom macros were developed in Image-Pro Analyzer to automate tiling and assembly of individual limb sections into a single composite image and then rendered using the Image-Pro 3D constructor.

In Vivo Cell Cycle Reentry Assay

Cross-sections of the forelimb stump were acquired, stained and imaged as described above. Sections were stained for EdU incorporation, anti-chick tenascin-C, MF20 and DAPI. An area of interest within the mesoderm of the limb, excluding the dermis, was manually defined and the number of EdU+ cells in TN-rich and TN-poor regions was determined using the *Count/Size* tool in Image-Pro Analyzer. For each time point $n \geq 5$.

Cell Culture

Primary cultures of newt myoblasts were prepared from myofiber cultures using previously described methods (Kumar and Brockes, 2007). In short, forelimbs were amputated proximal to the elbow, the epidermis was removed and the limb was placed in a solution of 0.1% collagenase type IV (Sigma) in newt MEM [0.8X Minimum Essential Medium (MEM, 10370, Gibco), 1X Pen/Strep/Fungiezone (HyClone)]. After enzymatic digestion for 2.5 - 3 hrs in a water jacketed incubator at 25°C, 2.0% CO_2 (ThermoForma), the muscles were dissected away from the limb, placed in a fresh collagenase solution and triturated through a fire polished Pasteur pipet. To remove mononucleate cells and debris, the suspension was passed through a 100 μm cell strainer (BD Falcon). Myofibers were reconstituted in serum free newt MEM and plated. After the myofibers attached to the substrate, media was changed to newt growth medium [GM: 0.8X MEM, 10% fetal bovine serum (FBS, SV30014.03, HyClone), 2 mM L-glutamine (HyClone), 1X Pen/Strep/Fungiezone, 25 mM insulin (Sigma)] and cultures were incubated at 25°C, 2.0% CO_2. Muscle-derived mononucleate progenitor cells appeared after 5 - 7 days. Cells were expanded under subconfluent conditions and passaged 1:2 with 0.25% trypsin (HyClone). Newt myoblasts grown in high serum maintained an undifferentiated mononucleate phenotype over many passages as determined by Pax7 staining (Seale et al., 2000). Multinucleate myotubes were generated from confluent cultures by switching to a low serum differentiation medium [DM: 0.8X, 1% FBS, 0.4 mM L-glutamine, 1X Pen/Strep/Fungiezone, 2.5 mM insulin]. The muscle derived newt A1 cell line (Ferretti and Brockes, 1988) was cultured as described above. C2C12 mouse myoblasts (CRL-1772, ATCC) were expanded under subconfluent conditions in high serum growth media [Dulbecco's Modification of Eagles Medium (DMEM, 10-013-CV, Cellgro), 10% FBS, 2 mM L-glutamine, 1X Pen/Strep (HyClone)] at 37°C, 5.0% CO_2. Cell fusion was induced by switching confluent cultures to low serum differentiation medium [DMEM, 5% horse serum (SH3007403, HyClone), 0.4 mM L-glutamine, 1X Pen/Strep].

Assessing DNA Synthesis in Cultured Cells

Commercially available ECMs were diluted in newt MEM and were allowed to passively adsorb to multi-well tissue culture polystyrene dishes for a minimum of 1 hour then rinsed with PBS (Table S2). Wells were coated in quadruplicate for the DNA synthesis assay and in duplicate for the migration and fusion assays. Importantly, ECM-coated dishes were not

allowed to dry at any time before plating with cells. Successful coating was confirmed via IHC with respective antibodies. Polystyrene was coated with HA using a modification of a previously established protocol (Kujawa and Tepperman, 1983; Turley and Roth, 1979). Wells were incubated with a solution of 2.5 mg/mL N-(3-dimethylaminopropyl)-N'-ethylcarbodiimide hydrochloride (EDC, Sigma) and 0.5 mg/mL HA overnight at 25°C, 2.0% CO_2. EDC is typically used to functionalize HA by coupling an amine-containing molecule with the carboxyl group of HA through the formation of a peptide bond (Kuo et al., 1991). However, EDC can also form ester linkages between the carboxyl and hydroxyl side groups of HA, creating an insoluble network that precipitates onto polystyrene (Everaerts et al., 2008; Tomihata and Ikada, 1997). HA coating was verified by staining with HABP (data not shown). Wells were gently rinsed with water before plating with cells. Myoblasts were plated at subconfluent density (2.5×10^3 cells/cm^2 for newt cells and 5×10^3 for C2C12 cells) and cultured in GM for 48 hours. EdU was added to each well (final concentration of 1 μM) and after 3 hours cells were fixed, permeabilized and stained with AF488 azide and DAPI as described above. Twelve non-overlapping images were acquired for each well (28.8 mm^2 total) and cell counting was automated using custom macros developed in Image-Pro Analyzer.

In Vitro Cell Migration Assay

Myoblasts were plated in GM at the same subconfluent density as in the DNA synthesis assay. Primary newt myoblasts and A1 cells were imaged at 25°C, 2% CO_2 and C2C12 cells at 37°C, 5% CO_2 every 30 minutes for 19 hours on a Leica DMI6000 live cell microscope. The total travel distance of 40 cells for each experimental parameter was determined by manually tracking individual cells using Image-Pro Analyzer. For rapidly migrating cells on HA-coated substrate, $n \geq 8$.

In Vitro Myotube Fragmentation Assay

Primary newt myoblasts were cultured to confluence in GM and induced to fuse as described above. 2 – 3 days after switching to low serum DM, cells were trypsinized, filtered through a 40 μm mesh to remove mononucleate cells, reconstituted in GM and plated in triplicate on polystyrene coated with different ECM. Myotubes were imaged at 25°C, 2% CO_2 every hour for 136 hours on a Leica DMI6000. Only fragments that contained nuclei and were viable for more than 5 hours were counted as a positive fragmentation event. Using an Eppendorf FemtoJet, reporter constructs pXCarGFP3 (E. Amaya) and pCMV-H2AmCherry (Tol2kit, (Kwan et al., 2007)) were directly injected into individual myotubes to confirm cell fragmentation. After 24 hours, myotubes expressing both fluorescent proteins were selected and imaged for 70 hours as described.

In Vitro Myotube Fusion Assay

Primary newt myoblasts were plated in GM at a subconfluent density (2.5×10^3 cells/cm^2) and cultured to confluence. Fusion was induced by switching to low serum DM. 24 hours after onset of fusion, cells were fixed with -20°C methanol for 5 minutes and stained with MF20 (to identify differentiating myotubes), Pax7 (to identify undifferentiated satellite

cells) and DAPI. To quantify undifferentiated muscle progenitors, the percentage of MF20-/Pax7+ cells in at least three different frames was determined ($n \geq 320$ cells).

Statistical Analyses

Two-way ANOVA and Bonferroni's post hoc test were used to assess the effects of TN and regeneration time on DNA synthesis in regenerating newt limbs. One-way ANOVA and Tukey-Kramer's post hoc test were used to compare the effects of different matrices on *in vitro* DNA synthesis and migration of newt primary myoblasts, newt A1 cells and mouse C2C12 cells. For the cell migration assays, distances traveled by cells were $\log_{10}$-transformed to normalize variances before statistical analyses were performed.

Results

A common gene expression response indicates dramatic ECM remodeling in forelimb and hindlimb regeneration

To determine if distinct classes of genes orchestrate the recruitment, proliferation and subsequent re-differentiation of progenitor cells during tissue regeneration, we used microarray analysis to identify genes that were commonly expressed in both forelimbs and hindlimbs during regeneration. *TN* and *FN* mRNA were upregulated shortly after appendage amputation, whereas the α1 chains of *type I* and *type II collagen* were downregulated during the first 12 days postamputation (dpa) (Fig. 1; data not shown). *MMP3/10b* and *nCol*, a newt specific collagenase, were upregulated within the first 24 hours. While *MMP3/10b* gradually decreased with time, *nCol* displayed a bimodal expression in the forelimbs, consistent with previous reports (Vinarsky et al., 2005). In comparison to the day 0 control, *MMP13* expression initially dropped, but steadily increased between 3 and 21 dpa. The comparable expression profiles in forelimbs and hindlimbs suggest that early matrix remodeling is a conserved response during the regeneration process.

HA, TN and FN build a regeneration specific transitional matrix

To achieve a deeper understanding of the functional role the ECM plays in limb regeneration, we developed a spatiotemporal map of key ECM components. We determined the expression patterns of HA (red), TN (green) and FN (blue) during the first month of regeneration, the time window reflecting the most dramatic changes in expression (Fig 2). Sections of forelimbs harvested at defined time points revealed a dynamic distribution of all three matrix proteins (Figs. 2A – 2T). Reliable antibodies against HA are not available; therefore, we utilized biotinylated hyaluronic acid binding protein as a probe to specifically detect HA (Ripellino et al., 1985). To our knowledge, this is the first time that the HA expression pattern has been determined in the regenerating newt limb.

In the normal, unamputated limb, we found HA to be widely distributed, particularly within the skeletal muscle, periosteum and dermis (Fig. 2A). Within a week after amputation, HA was significantly upregulated in the tissues directly below the wound epidermis (Fig. 2B). By 14 to 21 dpa, HA was strongly expressed throughout the stump tissue, with the highest levels present in the dermis and at the interface between the blastema and stump tissue (Figs. 2C and D). We observed a downregulation of HA where cartilage condensations formed at

the distal end of the humerus (Fig. 2D, asterisk). By 28 dpa, HA expression decreased to a lower level overall except around the newly forming joints (Fig. 2E, arrows).

TN distribution was more discrete in the normal limb and localized to the tendons, myotendinous junctions, epithelia, periosteum and areas surrounding the glands in the dermis (Fig. 2F). Consistent with its mRNA profile (Fig. 1), TN protein was dramatically upregulated soon after amputation and by the end of the first week, had begun to infiltrate the stump tissue (Fig. 2G). Throughout blastemal growth, the undifferentiated progenitor cell mass was embedded within a TN-rich matrix. In addition, TN was highly expressed at the boundary between the wound epidermis and blastema (Figs. 2H and I). The distribution of TN became restricted as tissues differentiated, and was downregulated, along with HA, within condensing cartilage at 21 dpa (Fig. 2I, asterisk). Between 21 and 28 dpa, TN expression decreased globally, except within in the growth zone in the distal most regions of the limb under the wound epidermis (Figs. 2I and J).

During regeneration, FN revealed a more modest expression profile than HA and TN (Figs. 2K - O). At 7 dpa, FN was upregulated directly under the wound epidermis concomitant with HA and TN (Fig. 2L). FN expression increased within the dermis, along with HA (Fig. 2M). In the blastema, FN co-localized with TN in a layer between the blastema and the wound epidermis and was most strongly expressed in the progenitor cell mass (Figs. 2N and O). Unlike with HA and TN, we did not observe significant downregulation of FN within areas of cartilage condensation (Fig. 2N, asterisk and O).

During the first 21 dpa, all three matrices were highly expressed around the distal ends of regenerating brachial nerves and skeletal muscle fibers and at the interface between the dermis and limb mesenchyme. HA, TN and FN were detected in the periosteum/perichondrium at all time points. Our data demonstrate that upon amputation, a transitional matrix rich in HA, TN and FN, is expressed within both distinct and overlapping domains in the stump and regeneration blastema.

Changes in ECM distribution and DNA synthesis correlate with tissue reorganization

To determine the spatial distribution of the transitional ECM with respect to skeletal muscle during regeneration, adjacent sections were stained with MF20 (red), an antibody against striated muscle-specific light meromyosin (Figs. 2U - Y and S1). In addition, the location of cells that were actively synthesizing DNA (white) was determined by injecting newts with EdU three hours before tissue harvest. One week after amputation, the skeletal muscle had considerably retracted away from the amputation plane (Figs. 2V and S1G). At 14 dpa, regions of isolated MF20 expression suggest muscle fragmentation (Figs. 2W and S1H, arrowhead). The severed skeletal muscle began to regenerate toward the amputation plane by 21 dpa (Figs. 2X and S1I). At 28 dpa, differentiated skeletal muscle was present throughout the regenerating limb and appeared to be derived from both extension of injured muscle in the stump and *de novo* formation at distal locations in the regenerate. (Figs. 2Y and S1J arrowhead).

In line with previous reports, we detected few EdU+ cells within the normal limb mesodermal tissues, whereas a considerable number were located in the epidermis of normal

and regenerating limbs with the notable exception of the newly formed wound epidermis (Figs. 2U - Y and S1K - O) (Hay and Fischman, 1961). The number of EdU+ cells within mesodermal tissues increased substantially during the first 7 dpa, and by 14 dpa large regions of the stump supported DNA synthesis (Figs. 2V, 2W, S1L and S1M). At 21 dpa, EdU incorporation was most prominent within the transition from the stump to the regenerate and the distal areas of the blastema (Figs. 2X and S1N). As the tissues began to differentiate, the majority of EdU+ cells were distributed throughout the mesenchyme (Figs. 2Y and S1O). Notably, the timing and distribution of EdU incorporation shown in Figures 2 and S1 directly correlate with previously reported mitotic indices measured during newt forelimb blastema formation (Chalkley, 1954).

Direct comparison of changes in matrix distribution in context with skeletal muscle during regeneration revealed new insight into the potential functions of ECM molecules (Figs. 2 and S2). In intact muscle, HA and FN were present in the interstitial matrix, whereas TN was restricted to the tendons and few EdU+ cells were present outside of the epidermis (Figs. 2, S2A and S2A', asterisk). By 7 dpa, myofibers became surrounded by a matrix rich in HA, TN and FN (Figs. 2, S2B and S2B'). Areas positive for HA and FN indicated where myofibers had degenerated, leaving behind their basement membrane and the interstitial ECM (Fig. S2B, arrowheads). At 21 dpa, cells actively synthesizing DNA appeared to be migrating away from the regenerating myofibers into the transitional matrix and some of these nuclei were positive for both EdU and Pax7, a transcription factor that identifies skeletal muscle satellite cells (Figs. S2D, S2D' and S3) (Seale et al., 2000). Of note, Pax7+ cells were found outside the confines of the residual basement membrane in the stump distal to the amputation plane, suggesting that satellite cells were migrating into the blastema (Fig. S3A' – S3D', arrows). The high expression of HA, TN and FN proximal to the regenerating myofibers persisted through 28 dpa (Figs. 2, S2C – S2D'). However, HA and TN were downregulated in areas where skeletal muscle had differentiated in the distal autopod, while FN showed persistent expression (Figs. 2, S2E and S2E', arrowhead).

Changes in ECM distribution and DNA synthesis correlated with tissue reorganization in the stump and newly differentiating tissues in the regenerate (Fig. 3A and 3A'). In a 28 dpa regenerate, HA and TN were downregulated in the autopod concomitant with areas of muscle differentiation (Fig. 3B and 3B'). HA expression within the chondrocyte pericellular matrix of the regenerating ulna decreased along the proximal-distal axis, correlating with a decline in EdU+ incorporation (Fig. 3C and 3C'). TN was upregulated within the regenerating brachial nerves, and EdU+ cells were localized to these TN-rich areas (Fig. 3D and 3D'). The data presented in Figs. 2 and 3 indicate that the transitional matrix correlates with, and possibly influences, DNA synthesis, proliferation and differentiation.

The TN-rich transitional matrix infiltrates damaged skeletal muscle and supports muscle fragmentation and cell cycle reentry

The MF20+ skeletal muscle fragments seen at 14 dpa may be indicative of muscle fragmentation (Figs. 2E, S1B and S2C'). Alternatively, it is possible that the fragments represent intact myofibers that extend out of the image plane. To address this question, a series of adjacent sections encompassing the full thickness of the limb was compiled and

reconstructed in 3D (Fig. 4). TN expression was used as an indicator of the regenerative transitional matrix (Figs. 2B and S2). In the intact limb, 3D rendering confirmed that TN was limited to the epidermis, tendons and periosteum (Fig. 4 and Video 1). After 21 dpa, TN was highly expressed throughout the undifferentiated cell mass of the early blastema and infiltrated the differentiated muscle in the stump. At this time, the skeletal muscle had retracted from the amputation plane but we could detect MF20+ fragments at the distal end of the muscle, suggesting that myofiber fragmentation had occured (Figs. 4 and S4 and Videos 2 and 3). By 28 dpa, skeletal muscle from the stump had regenerated through the amputation plane within the TN-rich environment and isolated groups of MF20+ cells could be identified in the blastema (Fig. 4 and Video 4). The 35 dpa regenerate also revealed evidence of distinct groups of MF20 expressing cells in the autopod in addition to a continuum of old and regenerated muscle from the stump (Fig. 4 and Video 5). The 28 and 35 dpa 3D reconstructions suggest that new muscle in the limb regenerate is derived both directly from existing severed muscle and through *de novo* generation at more distal locations. Thus, the 3D renderings confirmed that, embedded within a TN-rich matrix, the musculature of the limb not only retracts from the amputation plane and fragments into smaller groups of myofibers and/or myoblasts, but also rebuilds the severed muscle across the amputation plane. These data reveal that muscle formation may be the result of migration and proliferation of committed myogenic progenitor cells or, alternatively, *de novo* generation from multipotent blastema cells.

To determine whether the invading transitional matrix is in direct contact with the skeletal muscle myofibers, we stained cross-sections of regenerating limbs for type IV collagen (white), MF20 (red), TN (green) and DAPI (blue). At 3 dpa, the humeroantebrachialis muscle was composed of both intact and degenerating myofibers (Fig. 5A). Magnification of the uninjured area revealed tightly packed myofibers with peripheral nuclei ensheathed by type IV collagen and minimal TN reactivity (Fig. 5B). In contrast, damaged myofibers within the same muscle showed a significant influx of cells and high expression of TN within the disrupted basement membrane (Fig. 5C).

To provide further evidence that the transitional matrix supports cell proliferation *in vivo*, we determined the distribution of EdU+ cells with respect to TN expression within cross-sections of regenerating stumps proximal to the amputation plane. Consistent with the longitudinal sections (Figs. 2 and S1), intact muscle expressed very little TN (green) and the majority of EdU+ cells (white) were localized to the epidermis (data not shown). By 3 dpa, TN was upregulated within the skeletal muscle (red); however, TN expression preceded the induction of DNA synthesis in the stump, given that we observed no cell cycle reentry until 5 dpa (Fig. 5E – 5G). Quantification of the percentage of EdU+ nuclei present within TN-rich and TN-free areas of mesodermally derived tissues demonstrated that EdU incorporation was strongly associated with TN expression ($p < 0.0001$, Fig. 5H). These *in vivo* data suggest that the infiltrating transitional matrix, as indicated by the expression of TN, defines an environment that supports both DNA synthesis and fragmentation.

Changes in ECM selectively influence DNA synthesis, migration, fragmentation and differentiation

To directly test whether the transitional matrix has instructive properties on the cells in the damaged tissue, primary newt myoblasts (PM) were plated on tissue culture polystyrene coated with different components of the transitional matrix (HA, TN and FN) as well as matrices traditionally used for the culture of skeletal muscle derived cells (Matrigel, laminin and type I collagen) (Table S2). As a basis for comparison, we included the newt A1 skeletal muscle derived cell line (Ferretti and Brockes, 1988) and the murine C2C12 muscle cell line. All data were normalized to the uncoated polystyrene control. ECMs were passively adsorbed onto the polystyrene except for HA, which does not readily adhere to most cell culture surfaces. Therefore, we developed a method using N-(3-dimethylaminopropyl)-N'-ethylcarbodiimide hydrochloride to cross-link HA overnight, resulting in the robust precipitation and adsorption of HA onto the substrate.

The induction of cell proliferation is critical for the generation of progenitor cells within the blastema. Therefore, we first determined the influence of substrate coating on DNA synthesis of the different cell lines. After 48 hours of culture at subconfluent conditions, the percentages of EdU incorporation for PM, A1 and C2C12 cells on uncoated polystyrene were 28.1% ± 2.0%, 30.4% ± 3.0% and 46.6% ± 4.1%, respectively (n = 4 wells ± SD). Matrigel and laminin significantly stimulated DNA synthesis in all lines tested ($p < 0.05$), increasing the number of EdU+ cells by 18 – 93% depending on the substrate and cell type (Fig. 6). TN and FN increased EdU incorporation in PM and A1 cells by 32 – 84% ($p < 0.01$), enhancing DNA synthesis by approximately the same magnitude as seen *in vivo* (Figure 5H). Interestingly, HA inhibited EdU incorporation by PM cells ($p < 0.001$). In these cultures, DNA synthesis correlated with cell density, indicating that cell proliferation is affected by the matrix environment.

In addition to proliferation, cellular migration is also important for the correct distribution and concentration of progenitor cells during regeneration. To determine the influence of the ECM on cell migratory behavior, we performed *in vitro* time-lapse microscopy. Myoblasts were imaged every 30 minutes and the change in individual cell positions was recorded. The average distances PM, A1 and C2C12 cells migrated on uncoated polystyrene in 19 hours were 177.8 μm ± 14.2 μm, 104.4 μm ± 8.3 μm and 375.8 μm ± 27.4 μm, respectively (n = 40, ± SEM). Both newt and murine derived myoblasts migrated significantly farther on TN (190 – 264%) and laminin (185 – 272%) as compared to the control ($p < 0.01$, Fig. 7B, note logarithmic scale). Interestingly, we identified two distinct modes of migration on HA-coated dishes. The majority of cells demonstrated reduced migratory behavior in comparison to the uncoated control. However, a small population of phenotypically rounded cells (8.4% ± 2.5%, ± SEM) migrated approximately 10-fold farther than the control before slowing down and becoming more spindle shaped (794 – 2,646%, Fig. 7A and Video 6). While the rapidly migrating PMs could be part of the subset that are negative for Pax7, both the morphology of PMs after slowing down and the exhibition of this behavior by C2C12 cells (Blau et al., 1983), a subcloned population of C2 myoblasts, indicate that they belong to the myogenic lineage.

To test whether ECM composition could directly influence the fragmentation of *in vitro* derived newt multinuclear myotubes, we performed time-lapse microscopy (Fig. 8 and Video 7). HA and TN substantially promote myotube fragmentation when compared to FN, Matrigel, laminin and type I collagen (Fig. 8B). When plated on HA or TN, 33 – 38% of the myotubes fragmented without apparent fusion of adjacent myotubes. However, only 0 – 10% of myotubes fragmented on FN, Matrigel, laminin or type I collagen substrates, and adjacent myotubes fused at a rate of 24% and 37% when cultured on Matrigel or FN, respectively. Although the PM cultures were greater than 90% Pax7+, additional confirmation was needed to demonstrate fragmenting cells were indeed muscle derived. Therefore, multinucleate myotubes were individually co-injected with plasmid reporters that are expressed exclusively in cardiac and skeletal muscle cells (pXCarGFP3, green) (Breckenridge et al., 2001) or in cell nuclei (pCMV-H2AmCherry, red). Time-lapse microscopy demonstrated direct fragmentation of these labeled multinucleate myotubes and the resulting myocytes were viable for at least 24 hours after separation from the parent myotube (Fig. 8A, arrow and Video 7).

Progenitor cells in the regenerating blastema eventually differentiate into new tissues to reestablish functionality. To determine if the ECM can control differentiation of muscle-derived cells *in vitro*, primary newt myoblasts were plated on different matrices and allowed to become confluent. Undifferentiated myoblasts were identified by the expression of Pax7 (green) and differentiated myotubes that had begun to synthesize proteins of the contractile machinery were labeled with MF20 (red) (Fig. 9A). We observed enhanced myoblast fusion on FN, Matrigel and laminin, whereas HA inhibited differentiation to a level below that seen in the control. There was no significant difference between the percentage of Pax7+ cells on HA-coated polystyrene and the uncoated control, confirming that the MF20 negative cells maintained their myogenic phenotype (Fig. 9B).

In conclusion, our data reveal that key matrix components take on instructive roles during skeletal muscle regeneration, which can be interpreted by both amphibian and mammalian cells (Table 1). In response to tissue damage, a transitional matrix rich in HA, TN and FN creates an environment that supports cell cycle reentry and likely proliferation. HA and TN enhance myoblast migration and myofiber fragmentation while suppressing differentiation, thus facilitating the contribution of muscle derived cells to the blastema. At later regenerative stages myoblast fusion and muscle differentiation are supported by FN and laminin. Both *in vivo* and *in vitro* observations suggest that the spatially controlled downregulation of HA and TN is as essential for tissue differentiation as their initial upregulation is for the induction of regeneration.

Discussion

HA, TN and FN are integral components in the ECMs of embryonic development (Chiquet et al., 1981; Chiquet and Fambrough, 1984; Kosher et al., 1981; Matsumoto et al., 2009; Ros et al., 1995), wound healing (Ghosh et al., 2006; Longaker et al., 1991; Whitby and Ferguson, 1991) and regeneration (Contreras et al., 2009; Onda et al., 1991; Repesh et al., 1982; Tassava et al., 1996; Toole and Gross, 1971). Their coordinated expression may constitute an evolutionarily tested mechanism that creates an appropriate environment to

control tissue formation and restoration. The spatiotemporal distribution of these matrices with respect to each other and their direct effect on cellular behavior had not been previously investigated until now.

We used the regenerating newt forelimb as a model to map at high resolution the 3D distribution of HA, TN and FN with respect to skeletal muscle and cell cycle activity. Using time-lapse microscopy, we determined the functional properties of these matrices with regard to muscle proliferative potential, migration, fragmentation and fusion–all activities necessary for the formation of the regenerative blastema and subsequent tissue differentiation. We found that both amphibian and mammalian myoblasts displayed similar responses to ECM substrates, suggesting that the transitional matrix may provide a conserved code that could be interpreted by human cells to induce regenerative repair rather than scar formation following tissue damage.

Establishment of a regeneration specific transitional matrix

HA and FN are broadly distributed in the uninjured newt limb and envelop myofibers as part of the interstitial matrix. TN expression is more discrete and, in skeletal muscle, localized to the myotendinous junctions and tendons (Figs. 2, 4 and S2). Within 12-24 hours after amputation, epidermal cells migrate from the stump to form a specialized wound epidermis, the apical epidermal cap, which serves as an important signaling center thought to be functionally equivalent to the apical ectodermal ridge in the developing vertebrate limb (Rowe and Fallon, 1982; Thornton and Thornton, 1965). *TN* mRNA is upregulated over the first three days, and by 3 dpa the protein has visibly infiltrated the injured stump tissues (Figs. 1 and 5). *FN* is lower in abundance but by the end of the first week it is prominently expressed. It is not clear what type of cells are responsible for the synthesis of the regeneration-specific matrix during the initial stages, but eventually muscle derived and mesodermal progenitor blastema cells are induced to secrete HA, TN and FN (Gulati et al., 1983b; Huijbregts et al., 2001; Mescher and Munaim, 1986; Onda et al., 1990). Contemporaneous with synthesis of the transitional matrix, the expression of matrices typical of differentiated tissues (e.g. type I collagen and laminin) is suppressed, resulting in a dramatic change of the local environment. The immediate upregulation of specific MMPs likely functions to rapidly eliminate collagen and laminin, in addition to playing a role in the dynamic modulation of the regenerative matrix over time (Fig. 1) (Gulati et al., 1983a; Mailman and Dresden, 1976; Vinarsky et al., 2005).

Recruitment of progenitor cells for blastema formation

By the end of the first week, the distal stump tissues are imbedded within a matrix that is conducive for regeneration (Fig. 2). Our data reveal that the deposition of this transitional matrix precedes cell cycle reentry and that TN and FN are likely directly involved in stimulating cell proliferation (Figs. 2, 5 and 6). The interstitial matrix, now rich in HA, TN and FN, infiltrates the damaged basement membrane of the skeletal muscle, potentially changing the differentiated state of the muscle cell (Figs. 5 and 8). Myoblasts in an HA environment demonstrate reduced fusion and differentiation activities (Fig. 9), and a small, but significant percentage of myoblasts migrate more than 10-fold farther on HA-coated substrates than on uncoated polystyrene, confirming prior observations that HA influences

myoblast migration *in vivo* (Fig. 7) (Krenn et al., 1991). While the basement membrane component laminin enhances migration and EdU incorporation similar to TN, we found laminin also induces cell fusion (Figs. 6, 7 and 9). Therefore, the upregulation of HA and TN within the interstitial matrix of damaged muscle not only stimulates cell migration but may also act to inhibit the premature fusion of myoblasts as they migrate away from the damaged basement membrane into the blastema.

By two to three weeks, cells reenter the cell cycle and migrate distally out of the stump within a continuous transitional matrix network that stretches from the stump through the amputation plane into the blastema (Fig. 2). Our HA detection revealed lower expression in the blastema than in regions proximal to the amputation plane, corroborating earlier radiolabeling studies that found higher levels of HA in the distal stump as compared to the outgrowth of the regenerate (Toole and Gross, 1971). The presence of HA in the tissues proximal to the amputation plane likely functions to stimulate migration of progenitor cells into the blastema, while the limited expression of HA distal to the amputation plane may allow for progenitor cells to proliferate in the TN- and FN-rich blastema (Figs. 2 and 6).

Integration of 3D matrix distribution in the regenerating limb and live cell imaging suggests that an HA- and TN-rich environment induces fragmentation of differentiated myofibers (Figs. 2, 4, 8 and S4 and Videos 2, 3 and 7). Similarly, it has been shown that newt myotubes that have been labeled *in vitro* can fragment and contribute to tissues of different lineages when transplanted into a regenerating newt limb (Lo et al., 1993). In addition, the *in vivo* upregulation of HA and TN may promote satellite cell recruitment, given that Pax7+ cells were observed in the blastema and that these two ECM molecules enhance the *in vitro* migration of myoblasts (Figs. 2, 7 and S3). Thus, our *in vivo* and *in vitro* data indicate that multiple mechanisms may be involved in the generation of skeletal muscle progenitor cells, supporting previous findings that both satellite cells (Chen et al., 2006; Kragl et al., 2009; Morrison et al., 2010; Morrison et al., 2006) and fragmenting myofibers (Echeverri and Tanaka, 2002; Hay, 1959; Kumar et al., 2004; Lo et al., 1993; Namenwirth, 1974) can contribute to the blastema.

Differentiation and downregulation of the transitional matrix

The relatively homogeneous distribution of HA, TN and FN in the blastema changes by the end of the third week. HA and TN become downregulated in domains of cartilage condensation, confirming previous observations in limb regeneration as well as recapitulating ECM remodeling during cartilage development (Fig. 2S, asterisk) (Li et al., 2007; Mackie et al., 1987; Onda et al., 1991; Toole and Gross, 1971). A global downregulation of the transitional matrix has started by the fourth week postamputation, contemporaneous with multiple mesenchymal differentiation processes. For example, we find both *in vivo* and *in vitro* that skeletal muscle cells preferentially differentiate in areas with low levels of HA and TN (Figs. 2, 3, 9 and S2). This is consistent with studies that found tenascins and HA inhibit myoblast differentiation, while FN plays a role in guiding myotube formation (Chiquet et al., 1981; Hagios et al., 1999; Kujawa et al., 1986). Therefore, in the regenerating newt limb, local downregulation of HA and TN may be necessary for tissue differentiation to occur.

Isolated pockets of MF20+ cells in the distal autopod suggest that newly differentiated muscles can form *de novo* (Figs. 2 – 4 and Videos 3 and 4). These isolated myofibers may either arise from undifferentiated blastema cells or from migratory Pax7+ myoblasts from the stump (Fig. S3). Alternatively, these MF20+ cells may have been part of a single muscle anlagen that subsequently separated into individual muscles, a mechanism resembling muscle development in the chick limb (Kardon, 1998). Future investigations focusing on the transition between midbud and palette stage blastemas, in conjunction with high resolution 3D imaging of myogenic precursors and *in vivo* cell labeling, should reveal the true source of these isolated muscle masses.

During later stages of regeneration, TN expression defines the cartilage boundary and eventually becomes localized to the perichondrium/periosteum (Figs. 2 and 3). TN and HA are downregulated within domains of muscle differentiation; however, our 3D reconstructions revealed that regenerating skeletal muscle was actually surrounded by the TN-rich matrix at all times (Figs. 2 - 4). The persistence of TN at the interface of the developing perichondrium and skeletal muscles may be necessary for the connection of tendons to their presumptive muscles and cartilage/bone elements (Fig. 4) (Chiquet and Fambrough, 1984).

As the tissues differentiate, HA maintains robust expression within the regenerating joints in a distribution similar to joint cavitation in the developing chick limb (Figs. 2 and 3) (Pitsillides et al., 1995). While HA is downregulated as cartilage condenses, it remains within the pericellular matrix in the regenerating long bones and expression decreases along the proximodistal axis, correlating with a gradual decline in EdU+ cells (Figs. 2 and 3). A similar HA-dependent gradient in DNA synthesis was reported in the distal regions of the developing mouse humerus (Koziel et al., 2005). Moreover, a knock-out mouse model with hyaluronic acid synthase 2 conditionally removed from the limbs displayed defects in both growth plate organization and joint cavitation (Matsumoto et al., 2009). Combined with the previous reports, our data suggest that HA provides a critical extracellular environment for the establishment and/or maintenance of the growth plate and joints during limb development in the embryo and regeneration in the adult.

Additional complexity of the transitional matrix

The dynamic nature of the HA-, TN- and FN-rich transitional matrix is further enhanced by continuous remodeling of the ECM by specific MMPs that are expressed during the dedifferentiation and blastemal stages (Fig. 1) (Miyazaki et al., 1996; Park and Kim, 1999; Vinarsky et al., 2005; Yang and Bryant, 1994). MMP activity is required for normal newt limb regeneration (Vinarsky et al., 2005) and may function, in part, to degrade matrices associated with cell differentiation and scarring. For example, nCol and MMP3/10b cleave the native triple helical form of type I collagen, the primary protein found in connective tissue and an ECM molecule that promotes osteogenesis (Mizuno et al., 2000). We found expression of *α1 type I collagen*, which encodes the α1 chain of the type I collagen, downregulated during the early stages of limb regeneration concomitant with the upregulation of *nCol* and *MMP3/10b* (Fig. 1). This coordinated decrease in collagen synthesis and increase in degradation of existing collagen fibers likely allows the transitional

regenerative ECM to replace the collagen-based matrix of intact limb tissues. MMP13 has been reported in skeletal development (Inada et al., 2004), and we found its role to be recapitulated late in limb regeneration with strong expression between 12 and 21 dpa, correlating with cartilage formation in the distal humerus (Figs. 1, 2 and 3).

The transitional matrix in regenerative medicine

As a therapy for muscle diseases such as Duchenne Muscular Dystrophy, muscle progenitor cell implantation has been investigated, but in many cases, this treatment is hindered by limited survival and migration of the implanted cells (Bouchentouf et al., 2006). However, recent studies discovered that the induction of fiber damage by injury or exercise improves proliferation and migration of implanted myogenic cells during muscle repair (Ambrosio et al., 2009; Bouchentouf et al., 2006; Sherwood et al., 2004). In this context, it is of great interest that the expression of TN within the interstitial ECM of these damaged muscle fibers was significantly increased (Crameri et al., 2007; Fluck et al., 2003; Huijbregts et al., 2001). In line with our findings, an increase in HA and TN within the interstitial matrix induced by myofiber damage may enhance myoblast proliferation and migration while inhibiting premature fusion, allowing for more extensive repair of the musculature. Nevertheless, attempts to engineer replacements for skeletal muscle defects tend to rely upon exogenous scaffolding composed of either inert polymers or ECM typical of the differentiated state, which promotes fusion, reduces cell proliferation and ultimately results in limited functionality (Conconi et al., 2005; Kin et al., 2007; Merritt et al., 2010).

The results presented here indicate that additional ECM components deserve attention in ongoing efforts to enhance regenerative repair in humans. Considering the apparent conservation of ECM function on cell behavior in both amphibians and mammals, as well as between developmental and regenerative processes, the transitional matrix of the regenerating newt limb may provide a template to engineer biomimetic matrices that promote regenerative rather than scar-forming responses in humans.

Supplementary Material

Refer to Web version on PubMed Central for supplementary material.

Acknowledgments

The authors thank Dr. E. Amaya for sharing the pXCarGFP3 reporter plasmid. We are grateful to Dr. C. Huppenbauer and M. Tjepkema of W. Nuhsbaum Inc., N. Swentko of Intavis Inc., and Donald Atkinson for expert technical support. In addition, we would like to thank S. Mercer, Drs. R. Sadleir and L. Larkin for critical reading of the manuscript, and all members of the Simon laboratory for helpful discussions. This work was supported by DARPA, Restorative Injury Repair BAA04-12 Addendum B (H.-G. Simon and S. Odelberg), Searle Funds at The Chicago Community Trust (H.-G. Simon), and NIH T90 Regenerative Medicine Training Program (S. Calve).

References

Alvarado AS. Regeneration in the metazoans: Why does it happen? BioEssays. 2000; 22:578–590. [PubMed: 10842312]

Ambrosio F, Ferrari RJ, Fitzgerald GK, Carvell G, Boninger ML, Huard J. Functional overloading of dystrophic mice enhances muscle-derived stem cell contribution to muscle contractile capacity. Arch. Phys. Med. Rehab. 2009; 90:66–73.

Blau HM, Chiu CP, Webster C. Cytoplasmic activation of human nuclear genes in stable heterocaryons. Cell. 1983; 32:1171–80. [PubMed: 6839359]

Boonen KJM, Rosaria-Chak KY, Baaijens FPT, van der Schaft DWJ, Post MJ. Essential environmental cues from the satellite cell niche: Optimizing proliferation and differentiation. Am. J. Physiol.-Cell Ph. 2009; 296:C1338–C1345.

Bouchentouf M, Benabdallah BF, Mills P, Tremblay JP. Exercise improves the success of myoblast transplantation in *mdx* mice. Neuromuscular Disord. 2006; 16:518–529.

Breckenridge RA, Mohun TJ, Amaya E. A role for BMP signalling in heart looping morphogenesis in *Xenopus*. Dev. Biol. 2001; 232:191–203. [PubMed: 11254357]

Calve, S.; Simon, HG. Extracellular control of limb regeneration.. In: Arruda, EM.; Garikipati, K., editors. IUTAM Symposium on Cellular, Molecular and Tissue Mechanics. Springer; Netherlands: 2010. p. 257-266.

Carlson BM. Regeneration of a limb muscle in axolotl from minced fragments. Anat. Rec. 1970; 166:423–434. [PubMed: 5436847]

Chalkley DT. A quantitative histological analysis of forelimb regeneration in *Triturus Viridescens*. J. Morphol. 1954; 94:21–70.

Chen Y, Lin GF, Slack JMW. Control of muscle regeneration in the *Xenopus* tadpole tail by Pax7. Development. 2006; 133:2303–2313. [PubMed: 16687446]

Chiquet M, Eppenberger HM, Turner DC. Muscle morphogenesis: Evidence for an organizing function of exogenous fibronectin. Dev. Biol. 1981; 88:220–235. [PubMed: 7030825]

Chiquet M, Fambrough DM. Chick myotendinous antigen. I. A monoclonal antibody as a marker for tendon and muscle morphogenesis. J. Cell Biol. 1984; 98:1926–1936. [PubMed: 6725406]

Conconi MT, De Coppi P, Bellini S, Zara G, Sabatti M, Marzaro M, Zanon GF, Gamba PG, Parnigotto PP, Nussdorfer GG. Homologous muscle acellular matrix seeded with autologous myoblasts as a tissue-engineering approach to abdominal wall-defect repair. Biomaterials. 2005; 26:2567–2574. [PubMed: 15585259]

Contreras EG, Gaete M, Sanchez N, Carrasco H, Larrain J. Early requirement of hyaluronan for tail regeneration in *Xenopus* tadpoles. Development. 2009; 136:2987–2996. [PubMed: 19666825]

Crameri RM, Aagaard P, Qvortrup K, Langberg H, Olesen J, Kjaer M. Myofibre damage in human skeletal muscle: Effects of electrical stimulation versus voluntary contraction. J. Physiol.-London. 2007; 583:365–380. [PubMed: 17584833]

Donaldson DJ, Mahan JT, Yang H, Crossin KL. Tenascin localization in skin wounds of the adult newt *Notophthalmus viridescens*. Anat. Rec. 1991; 230:451–459. [PubMed: 1718188]

Echeverri K, Tanaka EM. Ectoderm to mesoderm lineage switching during axolotl tail regeneration. Science. 2002; 298:1993–1996. [PubMed: 12471259]

Epperlein HH, Radomski N, Wonka F, Walther P, Wilsch M, Muller M, Schwarz H. Immunohistochemical demonstration of hyaluronan and its possible involvement in axolotl neural crest cell migration. J. Struct. Biol. 2000; 132:19–32. [PubMed: 11121304]

Everaerts F, Torrianni M, Hendriks M, Feijen J. Biomechanical properties of carbodiimide crosslinked collagen: Influence of the formation of ester crosslinks. J. Biomed. Mater. Res. A. 2008; 85A:547–555. [PubMed: 17729260]

Ferretti P, Brockes JP. Culture of newt cells from different tissues and their expression of a regeneration-associated antigen. J. Exp. Zool. 1988; 247:77–91. [PubMed: 3183586]

Fluck M, Chiquet M, Schmutz S, Mayet-Sornay MH, Desplanches D. Reloading of atrophied rat soleus muscle induces tenascin-C expression around damaged muscle fibers. Am. J. Physiol.-R. 2003; 284:R792–R801.

Ghosh K, Ren XD, Shu XZ, Prestwich GD, Clark RAF. Fibronectin functional domains coupled to hyaluronan stimulate adult human dermal fibroblast responses critical for wound healing. Tissue Eng. 2006; 12:601–613. [PubMed: 16579693]

Goetsch SC, Hawke TJ, Gallardo TD, Richardson JA, Garry DJ. Transcriptional profiling and regulation of the extracellular matrix during muscle regeneration. Physiol. Genomics. 2003; 14:261–271. [PubMed: 12799472]

Grounds, MD. Complexity of extracellular matrix and skeletal muscle regeneration.. In: Schiaffino, S.; Partridge, T., editors. Skeletal Muscle Repair and Regeneration. Springer; Netherlands: 2008. p. 269-301.

Gulati AK, Reddi AH, Zalewski AA. Changes in the basement membrane zone components during skeletal muscle fiber degeneration and regeneration. J. Cell Biol. 1983a; 97:957–962. [PubMed: 6225786]

Gulati AK, Zalewski AA, Reddi AH. An immunofluorescent study of the distribution of fibronectin and laminin during limb regeneration in the adult newt. Dev. Biol. 1983b; 96:355–365. [PubMed: 6339298]

Hagios C, Brown-Luedi M, Chiquet-Ehrismann R. Tenascin-Y, a component of distinctive connective tissues, supports muscle cell growth. Exp. Cell Res. 1999; 253:607–617. [PubMed: 10585284]

Hay ED. Electron microscopic observations of muscle dedifferentiation in regenerating *Amblystoma* limbs. Dev. Biol. 1959; 1:555–585.

Hay ED, Fischman DA. Origin of the blastema in regenerating limbs of newt *Triturus viridescens*. An autoradiographic study using tritiated thymidine to follow cell proliferation and migration. Dev. Biol. 1961; 3:26–59. [PubMed: 13712434]

Huijbregts J, White JD, Grounds MD. The absence of MyoD in regenerating skeletal muscle affects the expression pattern of basement membrane, interstitial matrix and integrin molecules that is consistent with delayed myotube formation. Acta Histochem. 2001; 103:379–396. [PubMed: 11700944]

Hurme T, Kalimo H. Adhesion in skeletal muscle during regeneration. Muscle Nerve. 1992; 15:482–489. [PubMed: 1373471]

Inada M, Wang YM, Byrne MH, Rahman MU, Miyaura C, Lopez-Otin C, Krane SM. Critical roles for collagenase-3 (Mmp13) in development of growth and in endochondral plate cartilage ossification. Proc. Natl. Acad. Sci. U. S. A. 2004; 101:17192–17197. [PubMed: 15563592]

Iten LE, Bryant SV. Forelimb regeneration from different levels of amputation in newt, *Notophthalmus viridescens*: Length, rate, and stages. Roux Arch Dev Biol. 1973; 173:263–282.

Kardon G. Muscle and tendon morphogenesis in the avian hind limb. Development. 1998; 125:4019–4032. [PubMed: 9735363]

Kin S, Hagiwara A, Nakase Y, Kuriu Y, Nakashima S, Yoshikawa T, Sakakura C, Otsuji E, Nakamura T, Yamagishi H. Regeneration of skeletal muscle using *in situ* tissue engineering on an acellular collagen sponge scaffold in a rabbit model. ASAIO J. 2007; 53:506–513. [PubMed: 17667240]

Kosher RA, Savage MP, Walker KH. A gradation of hyaluronate accumulation along the proximodistal axis of the embryonic chick limb bud. J. Embryol. Exp. Morphol. 1981; 63:85–98. [PubMed: 7310297]

Koziel L, Wuelling M, Schneider S, Vortkamp A. Gli3 acts as a repressor downstream of Ihh in regulating two distinct steps of chondrocyte differentiation. Development. 2005; 132:5249–5260. [PubMed: 16284117]

Kragl M, Knapp D, Nacu E, Khattak S, Maden M, Epperlein HH, Tanaka EM. Cells keep a memory of their tissue origin during axolotl limb regeneration. Nature. 2009; 460:60–69. [PubMed: 19571878]

Krenn V, Brandsaberi B, Wachtler F. Hyaluronic acid influences the migration of myoblasts within the avian embryonic wing bud. Am. J. Anat. 1991; 192:400–406. [PubMed: 1781449]

Kujawa MJ, Pechak DG, Fiszman MY, Caplan AI. Hyaluronic acid bonded to cell culture surfaces inhibits the program of myogenesis. Dev. Biol. 1986; 113:10–16. [PubMed: 3943658]

Kujawa MJ, Tepperman K. Culturing chick muscle cells on glycosaminoglycan substrates: Attachment and differentiation. Dev. Biol. 1983; 99:277–286. [PubMed: 6413281]

Kumar A, Brockes JP. Preparation of cultured myofibers from larval salamander limbs for cellular plasticity studies. Nat. Protoc. 2007; 2:939–947. [PubMed: 17446893]

Kumar A, Velloso CP, Imokawa Y, Brockes JP. Plasticity of retrovirus-labelled myotubes in the newt limb regeneration blastema. Dev. Biol. 2000; 218:125–36. [PubMed: 10656757]

Kumar A, Velloso CP, Imokawa Y, Brockes JP. The regenerative plasticity of isolated urodele myofibers and its dependence on *Msx1*. PLoS Biol. 2004; 2:1168–1176.

Kuo JW, Swann DA, Prestwich GD. Chemical modification of hyaluronic acid by carbodiimides. Bioconjugate Chem. 1991; 2:232–241.

Kwan KM, Fujimoto E, Grabher C, Mangum BD, Hardy ME, Campbell DS, Parant JM, Yost HJ, Kanki JP, Chien CB. The Tol2kit: A multisite gateway-based construction kit for *Tol2* transposon transgenesis constructs. Dev. Dyn. 2007; 236:3088–3099. [PubMed: 17937395]

Li YC, Toole BP, Dealy CN, Kosher RA. Hyaluronan in limb morphogenesis. Dev. Biol. 2007; 305:411–420. [PubMed: 17362908]

Lo DC, Allen F, Brockes JP. Reversal of muscle differentiation during urodele limb regeneration. Proc. Natl. Acad. Sci. U. S. A. 1993; 90:7230–7234. [PubMed: 8346239]

Longaker MT, Chiu ES, Adzick NS, Stern M, Harrison MR, Stern R. Studies in fetal wound healing. V. A prolonged presence of hyaluronic acid characterizes fetal wound fluid. Ann. Surg. 1991; 213:292–296. [PubMed: 2009010]

Macfelda K, Kapeller B, Wilbacher I, Losert UM. Behavior of cardiomyocytes and skeletal muscle cells on different extracellular matrix components: Relevance for cardiac tissue engineering. Artif. Organs. 2007; 31:4–12. [PubMed: 17209955]

Mackie EJ, Thesleff I, Chiquet-Ehrismann R. Tenascin is associated with chondrogenic and osteogenic differentiation *in vivo* and promotes chondrogenesis *in vitro*. J. Cell Biol. 1987; 105:2569–2579. [PubMed: 2447094]

Mailman ML, Dresden MH. Collagen metabolism in the regenerating forelimb of *Notophthalmus viridescens*: Synthesis, accumulation, and maturation. Dev. Biol. 1976; 50:378–394. [PubMed: 1278591]

Maley MAL, Davies MJ, Grounds MD. Extracellular matrix, growth factors, genetics: Their influence on cell proliferation and myotube formation in primary cultures of adult mouse skeletal muscle. Exp. Cell Res. 1995; 219:169–179. [PubMed: 7628533]

Matsumoto K, Li YC, Jakuba C, Sugiyama Y, Sayo T, Okuno M, Dealy CN, Toole BP, Takeda J, Yamaguchi Y, Kosher RA. Conditional inactivation of *Has2* reveals a crucial role for hyaluronan in skeletal growth, patterning, chondrocyte maturation and joint formation in the developing limb. Development. 2009; 136:2825–2835. [PubMed: 19633173]

Merritt EK, Hammers DW, Tierney M, Suggs LJ, Walters TJ, Farrar RP. Functional assessment of skeletal muscle regeneration utilizing homologous extracellular matrix as scaffolding. Tissue Eng. Part A. 2010 In press.

Mescher AL, Munaim SI. Changes in the extracellular matrix and glycosaminoglycan synthesis during the initiation of regeneration in adult newt forelimbs. Anat. Rec. 1986; 214:424–431. [PubMed: 3706785]

Miyazaki K, Uchiyama K, Imokawa Y, Yoshizato K. Cloning and characterization of cDNAs for matrix metalloproteinases of regenerating newt limbs. Proc. Natl. Acad. Sci. U. S. A. 1996; 93:6819–24. [PubMed: 8692902]

Mizuno M, Fujisawa R, Kuboki Y. Type i collagen-induced osteoblastic differentiation of bone-marrow cells mediated by collagen-α2β1 integrin interaction. J. Cell. Physiol. 2000; 184:207–213. [PubMed: 10867645]

Morrison JI, Borg P, Simon A. Plasticity and recovery of skeletal muscle satellite cells during limb regeneration. FASEB Journal. 2010 In press.

Morrison JI, Loof S, He PP, Simon A. Salamander limb regeneration involves the activation of a multipotent skeletal muscle satellite cell population. J. Cell Biol. 2006; 172:433–440. [PubMed: 16449193]

Namenwirth M. The inheritance of cell differentiation during limb regeneration in the axolotl. Dev. Biol. 1974; 41:42–56. [PubMed: 4140121]

Oberpriller JO, Oberpriller JC. Response of the adult newt ventricle to injury. J. Exp. Zool. 1974; 187:249–259. [PubMed: 4813417]

Okita M, Yoshimura T, Nakano J, Motomura M, Eguchi K. Effects of reduced joint mobility on sarcomere length, collagen fibril arrangement in the endomysium, and hyaluronan in rat soleus muscle. J. Muscle Res. Cell M. 2004; 25:159–166.

Onda H, Goldhamer DJ, Tassava RA. An extracellular matrix molecule of newt and axolotl regenerating limb blastemas and embryonic limb buds: Immunological relationship of MT1 antigen with tenascin. Development. 1990; 108:657–668. [PubMed: 1696876]

Onda H, Poulin ML, Tassava RA, Chiu IM. Characterization of a newt tenascin cDNA and localization of tenascin mRNA during newt limb regeneration by *in situ* hybridization. Dev. Biol. 1991; 148:219–232. [PubMed: 1718799]

Park IS, Kim WS. Modulation of gelatinase activity correlates with the dedifferentiation profile of regenerating salamander limbs. Mol. Cells. 1999; 9:119–26. [PubMed: 10340464]

Pitsillides AA, Archer CW, Prehm P, Bayliss MT, Edwards JCS. Alterations in hyaluronan synthesis during developing joint cavitation. J. Histochem. Cytochem. 1995; 43:263–273. [PubMed: 7868856]

Repesh LA, Fitzgerald TJ, Furcht LT. Changes in the distribution of fibronectin during limb regeneration in newts using immunocytochemistry. Differentiation. 1982; 22:125–131. [PubMed: 6751911]

Ripellino JA, Klinger MM, Margolis RU, Margolis RK. The hyaluronic acid binding region as a specific probe for the localization of hyaluronic acid in tissue sections. Application to chick embryo and rat brain. J. Histochem. Cytochem. 1985; 33:1060–1066. [PubMed: 4045184]

Ros MA, Rivero FB, Hinchliffe JR, Hurle JM. Immunohistological and ultrastructural study of the developing tendons of the avian foot. Anat. Embryol. (Berl). 1995; 192:483–496. [PubMed: 8751106]

Rowe DA, Fallon JF. The proximodistal determination of skeletal parts in the developing chick leg. J. Embryol. Exp. Morphol. 1982; 68:1–7. [PubMed: 7108415]

Salic A, Mitchison TJ. A chemical method for fast and sensitive detection of DNA synthesis *in vivo*. Proc. Natl. Acad. Sci. U. S. A. 2008; 105:2415–2420. [PubMed: 18272492]

Sanes JR. The basement membrane/basal lamina of skeletal muscle. J. Biol. Chem. 2003; 278:12601–12604. [PubMed: 12556454]

Seale P, Sabourin LA, Girgis-Gabardo A, Mansouri A, Gruss P, Rudnicki MA. Pax7 is required for the specification of myogenic satellite cells. Cell. 2000; 102:777–786. [PubMed: 11030621]

Sherwood RI, Christensen JL, Conboy IM, Conboy MJ, Rando TA, Weissman IL, Wagers AJ. Isolation of adult mouse myogenic progenitors: Functional heterogeneity of cells within and engrafting skeletal muscle. Cell. 2004; 119:543–554. [PubMed: 15537543]

Tassava RA, Nace JD, Wei Y. Extracellular matrix protein turnover during salamander limb regeneration. Wound Repair Regen. 1996; 4:75–81. [PubMed: 17129351]

Thornton CS, Thornton MT. Regeneration of accessory limb parts following epidermal cap transplantation in urodeles. Experientia. 1965; 21:146–148. [PubMed: 5318741]

Tomihata K, Ikada Y. Crosslinking of hyaluronic acid with water soluble carbodiimide. J. Biomed. Mater. Res. 1997; 37:243–251. [PubMed: 9358318]

Toole BP, Gross J. The extracellular matrix of the regenerating newt limb: Synthesis and removal of hyaluronate prior to differentiation. Dev. Biol. 1971; 25:57–77. [PubMed: 5557969]

Turley EA, Roth S. Spontaneous glycosylation of glycosaminoglycan substrates by adherent fibroblasts. Cell. 1979; 17:109–115. [PubMed: 222473]

Vinarsky V, Atkinson DL, Stevenson TJ, Keating MT, Odelberg SJ. Normal newt limb regeneration requires matrix metalloproteinase function. Dev. Biol. 2005; 279:86–98. [PubMed: 15708560]

Vracko R, Benditt EP. Basal lamina: The scaffold for orderly cell replacement. Observations on regeneration of injured skeletal muscle fibers and capillaries. J. Cell Biol. 1972; 55:406–419. [PubMed: 5076781]

Whitby DJ, Ferguson MWJ. The extracellular matrix of lip wounds in fetal, neonatal and adult mice. Development. 1991; 112:651–668. [PubMed: 1724421]

Yang EV, Bryant SV. Developmental regulation of a matrix metalloproteinase during regeneration of axolotl appendages. Dev. Biol. 1994; 166:696–703. [PubMed: 7813787]

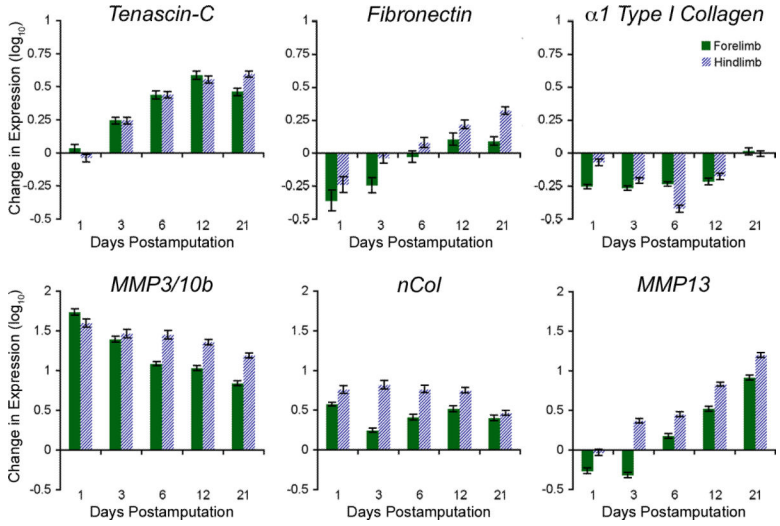

Figure 1. Key ECM and MMPs are differentially expressed during appendage regeneration

Differential expression of key genes reveals dramatic matrix remodeling during newt forelimb and hindlimb regeneration. Each time point was normalized to intact (day 0) expression levels and $\log_{10}$ transformed. Geometric means and standard deviations are shown. dpa = days postamputation.

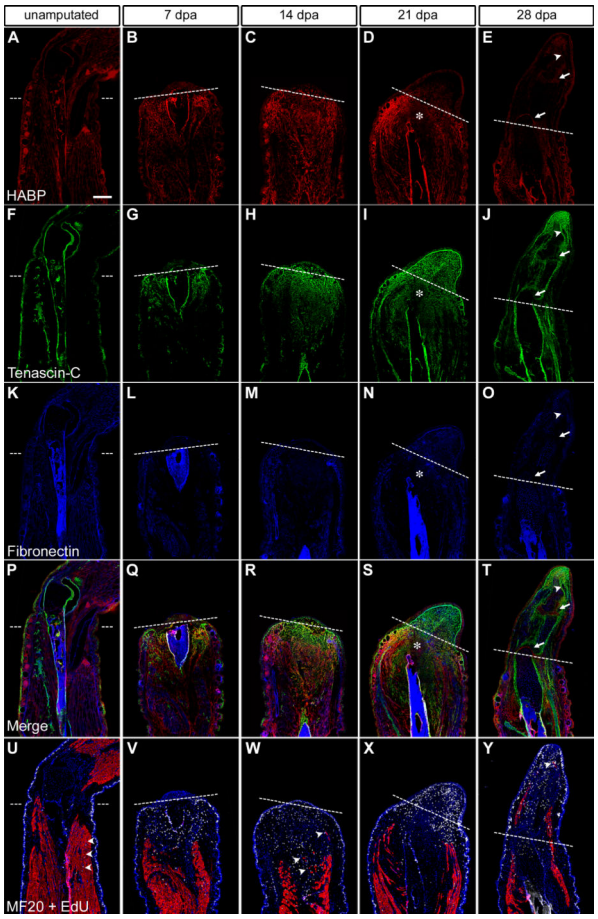

Figure 2. Limb amputation induces the deposition of a regeneration-specific transitional ECM

A - E: Hyaluronic acid (HA, red, indirectly labeled with hyaluronic acid binding protein, HABP), F – J: tenascin-C (TN, green), K – O: fibronectin (FN, blue) during forelimb regeneration at 7, 14, 21 and 28 days postamputation (dpa) in comparison to the normal, unamputated limb. HA was more highly expressed in the stump tissue and TN predominated the blastema; however, both were downregulated in areas of cartilage condensation (21 dpa, asterisk). Of note, HA was upregulated within the newly formed joints (28 dpa, arrows). U – Y: Adjacent sections were labeled to determine the distribution of the transitional ECM with respect to regenerating skeletal muscle (MF20 = red) and cells actively synthesizing DNA (EdU = white, DAPI = blue). In the unamputated limb, only a few EdU+ cells were detected outside of the epidermis (arrowheads). The number of EdU+ cells increased by 7 and 14 dpa and populated the same areas as the TN- and HA-rich matrix. Isolated fragments of MF20+ cells were present at 14 dpa (arrowheads). During the later stages, the majority of cells reentering the cell cycle were found distal to the amputation plane. TN and HA were downregulated within areas of skeletal muscle differentiation (28 dpa, arrowhead). Dashed line = amputation plane, dpa = days postamputation, bar = 400 μm. See also Figs. S1 and S2 for details on DNA synthesis and skeletal muscle regeneration.

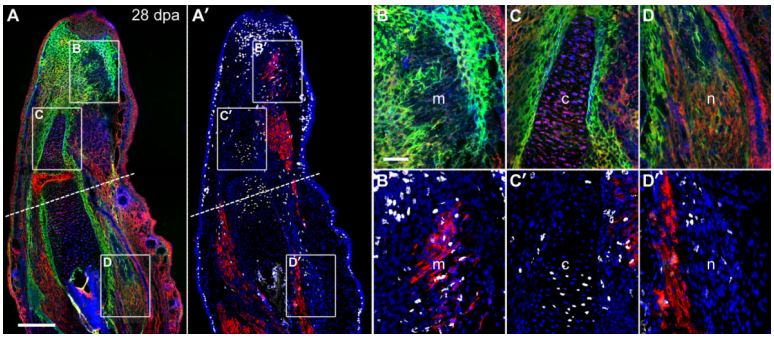

Figure 3. The regeneration-specific ECM is absent from differentiating muscle and bone

A and A’: Adjacent sections of a 28 dpa forelimb were stained for either components of the transitional matrix (TN = green, HA = red, FN = blue) or skeletal muscle and cells that had reentered the cell cycle (MF20 = red, EdU = white, DAPI = blue). B and B’: TN and HA were downregulated in areas of differentiating skeletal muscle (m) whereas FN expression remained constant. C and C’: HA was expressed in a proximal to distal gradient in the regenerating ulna correlating with EdU+ chondrocytes (c). D and D’: EdU+ cells were co-localized with TN in the regenerating brachial nerve (n). Dashed line = amputation plane, dpa = days postamputation. A and A’: bar = 400 μm. B – D’: bar = 100 μm.

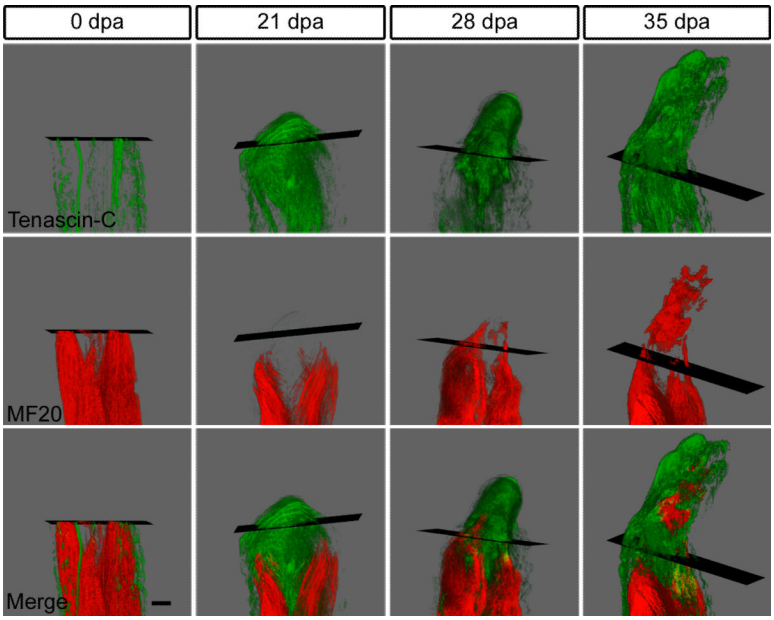

Figure 4. Regenerating skeletal muscle directly interacts with the transitional matrix

3D reconstruction of a regenerating forelimb at 0, 21, 28 and 35 dpa; 70 – 100 serial sections were imaged, assembled and rendered using ImageProPlus 6.1. See Videos 1 – 5. At 0 dpa, TN (green) was restricted to the tendons, periosteum, dermis and epidermis. A TN-rich matrix had infiltrated the stump at 21 dpa and skeletal muscle (MF20 = red) had regressed away from the amputation plane. By 28 dpa, the skeletal muscle regenerated through the amputation plane revealing both pockets of MF20 expression and extensions from stump musculature. Embedded within a TN-rich matrix, isolated MF20+ regions were found in the distal autopod. Black rectangle = amputation plane, dpa = days postamputation, bar = 400 μm.

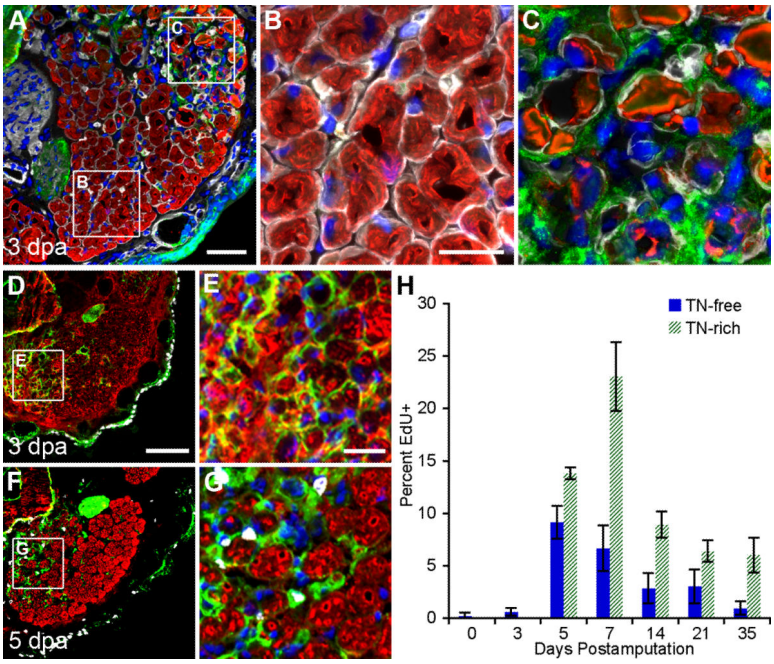

Figure 5. The transitional matrix infiltrates the basement membrane of degenerating myofibers and specifies regions of proliferative activity

A: Cross-section of 3 dpa forelimbs shows that the humeroantebrachialis has both intact and degenerating myofibers (MF20 = red, type IV collagen = white, TN = green, DAPI = blue). B: Uninjured fibers were surrounded by an intact basement membrane, defined by type IV collagen expression, and nuclei were predominantly found in the periphery of the myofiber syncytium. C: The basement membrane of degrading myofibers was infiltrated by a TN-rich matrix and centrally located nuclei. D - G: Cross-sections of regenerating limbs revealed inhomogeneous distribution of both the transitional matrix (TN = green) and EdU+ (white) cells within the humeroantebrachialis muscle (MF20 = red, skeletal muscle; DAPI = blue). Notably, increased TN expression is apparent at 3 dpa (D and E) and precedes the induction of DNA synthesis (F and G). H: EdU incorporation within the mesodermal tissues dramatically increased after 3 dpa, reaching a peak around 7 dpa, with significantly more cells synthesizing DNA in the TN-rich transitional matrix. Two-way ANOVA for Interaction ($p < 0.0001$), Matrix ($p < 0.0001$) and Time ($p < 0.0001$). Bonferroni's post hoc test revealed statistically significant differences in EdU incorporation between TN-rich and TN-free regions ($p < 0.001$). dpa = days post amputation A: bar = 100 μm. B and C: bar = 40 μm. D and F: bar = 200 μm. E and G: bar = 50 μm. H: Error bars = S.D., $n \geq 5$.

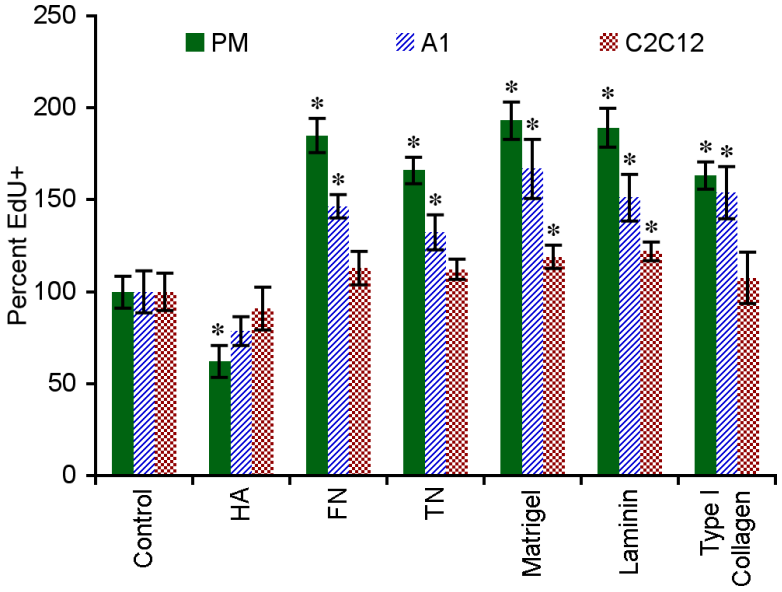

Figure 6. Matrix composition controls DNA synthesis

Primary newt myoblasts (PM), newt A1 and mouse C2C12 myoblast cell lines were cultured *in vitro* for 48 hours and the percentage of cells actively synthesizing DNA was determined by labeling for EdU incorporation. Data were normalized to uncoated control. Error bars = SD, $n \geq 4$. One-way ANOVA, $p < 0.0001$ for each cell type. Tukey-Kramer post-hoc tests revealed statistically significant differences between EdU incorporation on specific matrices versus the uncoated control (* $p < 0.05$).

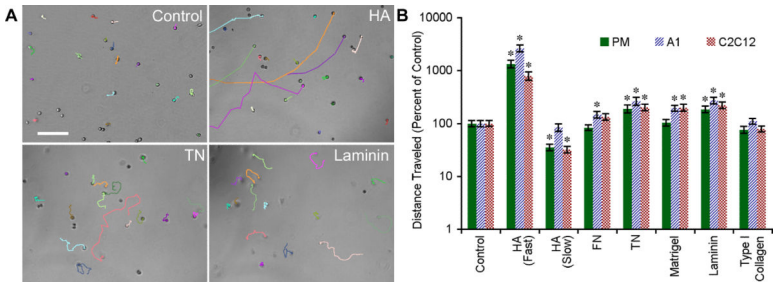

Figure 7. The ECM directs amphibian and murine myoblast migration

A: Myoblasts showed different migratory behavior on HA, TN, laminin and uncoated polystyrene. See Video 6. B: Migration of all cell lines was enhanced on TN and laminin, whereas cells plated on HA-coated substrates displayed a unique bimodal migration behavior with a subset of myoblasts migrating 10-fold farther than the control (note logarithmic scale of the y-axis). The rapidly migrating myoblasts eventually slowed down and took on the same spindle-shaped morphology displayed by the majority of cells plated on HA (arrowhead). Primary newt myoblasts (PM), newt A1 and mouse C2C12 cells were imaged for 19 hours and the total distance traveled was normalized to uncoated polystyrene. For all parameters $n = 40$ cells except HA (Fast) where $n \geq 8$, error bars = SD. One-way ANOVA, $p < 0.0001$ for each cell type. Tukey-Kramer post-hoc tests revealed statistically significant differences between myoblast migration on specific matrices versus the uncoated control (* $p < 0.05$).

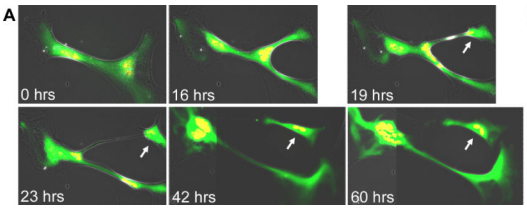

B

ECM coating	% fragment	% fusion	*n*
None	13	0	23
Hyaluronic Acid	38	0	13
Tenascin-C	33	0	24
Fibronectin	3	37	38
Matrigel	6	24	17
Laminin	10	0	21
Type I Collagen	0	4	23

Figure 8. Components of the transitional matrix induce myotube fragmentation

A: Live cell imaging identified viable cells budding off newt multinuclear parent myotubes when cultured on HA-coated polystyrene (arrow). Cells were co-injected with plasmids to identify differentiated muscle (pXCarGFP3, green) and nuclei (pCMV-H2AmCherry, red). Adjacent images were tiled (42 and 60 hrs) to illustrate viable fragmentation (see Video 7). B: Primary newt myotubes cultured for five days preferentially fragmented on HA and TN, whereas FN and Matrigel inhibited fragmentation and induced fusion.

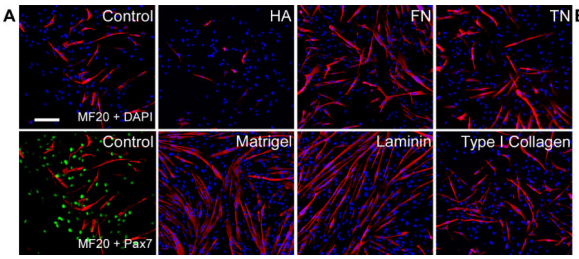

B

ECM Coating	% Pax7+/ MF20-
None	94.8 ± 0.7
Hyaluronic Acid	92.9 ± 2.6
Tenascin-C	90.9 ± 2.4
Fibronectin	89.5 ± 3.8
Matrigel	91.3 ± 1.6
Laminin	84.4 ± 4.9
Type I Collagen	85.0 ± 6.9

Figure 9. Basement membrane components enhance myoblast differentiation

A: Myoblast differentiation was defined by MF20+ staining (red) and undifferentiated muscle progenitors were identified by Pax7 expression (green). DAPI = blue, bar = 300 μm. B: Mononuclear undifferentiated cells (MF20-/Pax7+) on all substrates maintained their myogenic phenotype.

Table 1

Summary of the influence of the ECM on primary newt myoblasts *in vitro*.

ECM	Proliferation	Migration	Fusion	Fragmentation
Hyaluronic Acid	-	++/-	-	+
Tenascin-C	+	+	ns	+
Fibronectin	+	ns	+	-
Matrigel	+	ns	+	-
Laminin	+	+	+	ns
Type I Collagen	+	ns	ns	-

+ = enhanced compared to uncoated control, - = inhibited compared to uncoated control, ns = not significantly different from uncoated control